Percolation Images: Fractal Geometry Features for Brain Tumor Classification

Published Version:
Lumini, A., Roberto, G.F., Neves, L.A., Martins, A.S., do Nascimento, M.Z. (2024). Percolation Images: Fractal Geometry Features for Brain Tumor Classification. Switzerland : Springer [10.1007/978-3-031-47606-8_29].

Availability:
This version is available at: https://hdl.handle.net/11585/966228 since: 2024-03-12

Published:
DOI: http://doi.org/10.1007/978-3-031-47606-8_29

(Article begins on next page)

The Fractal Geometry of the Brain manuscript No.
(will be inserted by the editor)

Percolation images: fractal geometry features for brain tumor classification

Alessandra Lumini · Guilherme Freire Roberto · Leandro Alves Neves · Alessandro Santana Martins · Marcelo Zanchetta do Nascimento

Received: date / Accepted: date

Abstract Brain tumors detection is crucial for clinical diagnosis and efficient therapy. In this work, we propose a hybrid approach for brain tumor classification based both on fractal geometry features and deep learning. In our proposed framework, we adopt the concept of fractal geometry to generate a "percolation" image with the aim of highlighting important spatial properties in brain images. Then both the original and the percolation images are provided as input to a convolutional neural network to detect the tumor. Extensive experiments, carried out on a well-known benchmark dataset, indicate that using percolation images can help the system perform better.

Keywords Deep learning · Fractal features · Classification ensemble · Brain Tumors · Feature representations

Alessandra Lumini
Department of Computer Science and Engineering - University of Bologna, Via dell'Università 50, 47521, Cesena, FC, Italy.
E-mail: alessandra.lumini@unibo.it

Guilherme Freire Roberto
Institute of Mathematics and Computer Science (ICMC) - University of São Paulo (USP), Av. Trabalhador São-carlense, 400, 13566-590, São Carlos, SP, Brazil
E-mail: guilhermefroberto@gmail.com

Leandro Alves Neves
Department of Computer Science and Statistics (DCCE), São Paulo State University (UNESP), Rua Cristóvão Colombo, 2265, 15054-000, São José do Rio Preto, SP, Brazil.
E-mail: leandro.neves@unesp.br

Alessandro Santana Martins
Federal Institute of Triângulo Mineiro (IFTM), R. Belarmino Vilela Junqueira, S/N, 38305-200, Ituiutaba, MG, Brazil.
E-mail: alessandrosm2006@yahoo.com.br

Marcelo Zanchetta do Nascimento
Faculty of Computation (FACOM) - Federal University of Uberlândia (UFU), Avenida João Naves de Ávila, 2121, Bl.B, 38400-902, Uberlândia, MG, Brazil.
E-mail: marcelo.zanchetta@gmail.com

1 Introduction

The diagnosis, prognosis, and therapy of tumors all benefit from the automatic segmentation and categorization of medical pictures. Since brain tumor cancer is one of the fatal and most growing diseases, early detection of brain tumors allows a quicker response to therapy, which raises the survival percentage of patients. According to the WHO Classification of Tumors of the Central Nervous System (CNS) [1], CNS tumors can be classified into biologically and molecularly defined groups with characterize natural histories and distinguish tumor types and subtypes, with the goal of a better understanding of prognosis and optimal therapy for patients with specific CNS tumors. The most diffused types of brain tumor according to [2] are three: meningiomas, gliomas and pituitary. Meningiomas are benign tumor that originate from the thin membranes that surround the brain and spinal cord, specifically, from the cap cells of the arachnoid layer; anyway, grade III meningiomas, albeit rare, can be very aggressive, behaving like cancer. Gliomas are diffuse tumors that grow within the substance of the brain, they are quite aggressive, but if taken in the grade I can be cured by means of surgery. Pituitary adenomas arise from the pituitary gland, a gland in the skull base, which sometimes can involve the brain. The classification of brain tumors is carried out using several medical imaging techniques, anyway magnetic resonance imaging (MRI) is the most used technique to acquire information about tumors (tumor type, shape, size, location, etc.), necessary for their diagnosis. In MRI, pituitary adenomas and meningiomas appear as uniform intensities, while glioma tumor spreads over the glial cells of the brain and exhibits varying intensities. The location, shape, and size of these tumors, among other characteristics, differ from one tumor to another. Since manual segmentation and classification of brain tumors in a huge collection of medical images takes a lot of time and effort due to the large amount of information contained in each image, it is desired and useful to implement an automated detection and classification method for this task [3]. Two different problems can be addressed: (i) brain tumor segmentation (BTS) consists in differentiating tumor tissues from healthy ones, i.e. as a 2-class classification problem at a pixel-level, (ii) brain tumor classification (BTC) consists in classify a whole image according to the above cited taxonomy. Computer vision-based biomedical imaging technology has attracted more and more interest because it provides radiologists with recognition information for more effective treatment: the recent developments in deep neural network modeling have provided novel methods for the study, segmentation, and classification of brain malignancies [4, 5].

In recent years, numerous methods have been suggested for classifying or segmenting brain tumors in MRI. Published studies have evolved from using classical machine learning [6–9], where the classification pipeline includes a preprocessing stage designed for feature extraction and a classification stage, to the latest deep learning techniques, designed to enable computers to discover the features that best represent the data [10–20].

Among classical machine learning approaches, Sachdeva et al.[6] proposed a semi-automatic segmentation system which extracts 71 features using the intensity profile, the co-occurrence matrix, and Gabor functions; such features are coupled with standard classifiers: support vector machines (SVM) and artificial neural networks (ANN). Analogously, in [7] an approach for classifying brain tumors that utilized 10 characteristics and a back propagation network as the classifier is proposed, and in [8] fractal wavelet features are used with a self organizing map (SOM) classifier. Cheng et al. [9] extracted intensity histogram, gray-level co-occurrence matrix (GLCM), and bag-of-words (BoW) model-based features coupled with SVM classifier.

The advent of deep learning (DL) had profound influence on the design of medical imaging systems, and most recent research on brain tumors detection and classification is based on convolutional neural networks (CNN) and fully convolutional networks (FCN). DL methods have gained increasing amounts of attention due to their outstanding performance in many image classification tasks. However, using CNNs in the realm of medical imaging is difficult, due to the limited amount of data available for training which may lead the system to overfitting. A feasible solution consists in transfer-learning (TL), i.e. using DL models pre-trained on a large dataset and transfer learned knowledge to the target (small) dataset.

Several works in the recent literature have proposed transfer learning for brain tumor classification: the authors of [10] carried out extensive experiments comparing nine pre-trained DL models (InceptionResnetv2, Inceptionv3, Xception, Resnet18, Resnet50, Resnet101, Shufflenet, Densenet201 and Mobilenetv2) finding that InceptionResnetv2 outperforms the other DL models on Figshare [21] and Kaggle [22] datasets. While other models have been shown to work better in a clinic scenario [19]. Similarly, other authors [4][11] designed approaches for brain tumor classification using TL. Badža and Barjaktarovi [12] introduced a novel CNN architecture based on the modification of an existing pre-trained network: the proposed model showed a good generalization capability and good execution speed. Mzough et al.[13] proposed a 3D CNN model for glioma brain tumor categorization into 2 classes (low-grade and high-grade glioma): they suggested the use of a pre-processing strategy based on intensity normalization and adaptive contrast enhancement to overcome the data heterogeneity and studied the impact of the pre-processing and data augmentation on classification accuracy. Díaz-Pernas et al.[14] presented a fully automatic system for both tumor segmentation and classification: their model, a Deep Convolutional Neural Network that includes a multiscale approach, processed the images in three spatial scales along different processing pathways. An ad-hoc model for three-class brain tumor classification is proposed in [15], where a deep dense inception residual network is designed by customizing the output layer of InceptionResnetv2 with a deep dense network and a softmax layer. Another ad-hoc architecture is presented in [5] where a variant of EfficientNet is proposed with dense and drop-out layers added. Moreover data augmentation and min-max normalization is adopted to increase the contrast of tumor cells. The authors of [16] presented a multi-level attention mechanism network (MANet) which incorporates both spatial and cross-channel attention. A hybrid deep convolution neural network and deep watershed auto-encoder (CNN-DWA) model is proposed in [17] for tumor detection and segmentation. One problem of existing approaches is adaptability to different MRI machine: in order to improve flexibility, Alanazi et al. [18] suggested using a transfer-learning model strategy to categorize brain MRI data first in two classes (tumor/no tumor) then into the three tumor subclasses. Russo et al. [20] proposed a method based on a preprocessing phase for dealing with the problem of the lack of data standardization to adjust for different CNN models and MR machines. They dealt with tumor segmentation problem and showed the advantage of transforming input data using 3D spherical coordinates over the Cartesian-input trained model. In summary, as observed from the above research studies, the classification performance with DL approaches for brain MRI classification is significantly higher than with traditional ML techniques. However, traditional handcrafted features, which do not require a massive amount of data for training, can help solve this hard classification problem. In this paper we propose a method that mixes fractal geometry features and DL methods for brain MRI classification. The classification system proposed in this study is a hybrid solution that exploits handcrafted fractal feature (i.e. percolation) [23] to generate a "percolation image" that can highlight important spatial properties in brain MRI, in the next step both the original image and the percolation image are used to identify the tumors using a CNN. Our experiments, conducted on the well-known Figshare dataset [21], show that the use of percolation images can help improve the performance of the system.

2 Percolation

Handcrafted fractal features have been used for the classification of medical images since before most of the current state-of-the-art CNN models became available. These features still are a viable alternative for the quantification of images from datasets with a low number of samples. While Fractal Dimension (FD) and Lacunarity (LAC) have been applied in several studies as the main approaches for measuring fractal properties in images, percolation has recently shown to be another suitable way for obtaining features from medical images. Percolation is a physical concept regarding the transport of fluids through porous media. This concept has recently been applied to image feature extraction, where properties such as number of clusters and percolation occurrence can be measured.

One of the main studies on the application of percolation theory for tumor detection in medical images was published in [24], where the authors proposed that vascular growth of tumors can be described using percolation models. Recently, handcrafted percolation features have been used to quantify different types of histology images [23, 25], however the application of similar approaches to other types of medical images is limited. In [26], percolation theory was applied to evaluate topological images of the cortical activity, obtained from electroencephalograms; however, we found no recent applications of similar approaches for BTC in MRI.

In addition, an alternative approach for handling the obtained percolation features has been proposed. In [27], handcrafted fractal features are rearranged to form an RGB image, which is given as input to a CNN. However, the images generated from this approach do not retain spatial information. In this paper, we propose a technique to generate an image from the application of percolation concepts. The generated percolation image should be able to highlight important spatial properties in brain tumor's MRI, while also preserving spatial information.

3 Materials and Methods

3.1 Brain tumors datasets

Clinical situations typically allow the acquisition and availability of a limited number of brain MRI slices, each having a significant slice gap. With such a limited amount of data, creating a 3D model is challenging. Most of existing datasets for brain tumor detection are therefore based on 2D slices. In this study we perform a set of experiments on a publicly available brain MRI dataset (Figshare) [21]. Figshare is a collection of data from 233 patients, acquired in China from 2005 to 2010; it consists of 3064 images acquired in the three common views (sagittal, coronal, and axial) and split into three tumor classes: meningiomas (708 images), gliomas (1426 images), and pituitary tumors (930 images). Figure 1 shows examples of these three types of tumors. The images have a resolution of 512 $\times$ 512 pixels and have a segmentation mask, in which tumor pixels are labelled as 1 and healthy pixels as 0. The dataset does not include view labels, which were added manually for the purposes of this work. This dataset also provides a testing protocol based on five-fold cross-validation. Five-fold cross-validation (CV) is a testing protocol in which all data are randomly split into five folds, then the model is trained using four folds, while one fold is left for testing. This procedure is repeated five times, changing the test folder each time, and averaging the classification performance. In our case the split process is not random since the indices are given by the authors [9].

3.2 Dataset Pre-Processing

All the MRI images were pre-processed as proposed by [28], in order to remove noise and unwanted areas that negatively affect classification performance and cropped to a fixed size as required by DL approaches. The pre-processing procedure involves the following steps: (a) conversion to grayscale and slightly blurring, (b) thresholding the image, then perform a series of morphological

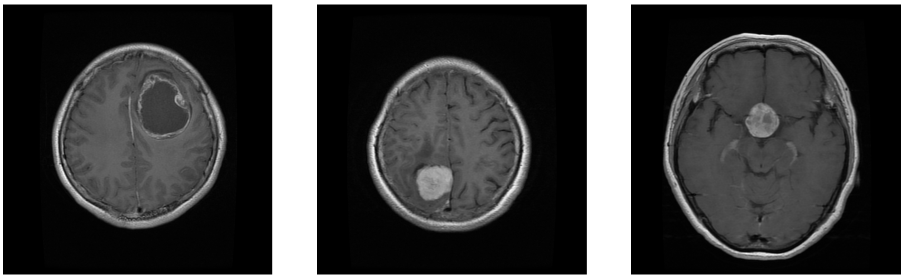

(a) (b) (c)

Fig. 1 Samples of images from the Figshare dataset: (a) Glioma; (b) Meningioma; (c) Pituitary.

erosions and dilations to remove any small regions of noise, (c) locating contours in thresholded image, then determine the most extreme points along the contour, (d) cropping the image using the most extreme points, pad to square (to avoid image stretching) and resizing to 352 $\times$ 352. Figure 2 shows an example of the pre-processing steps.

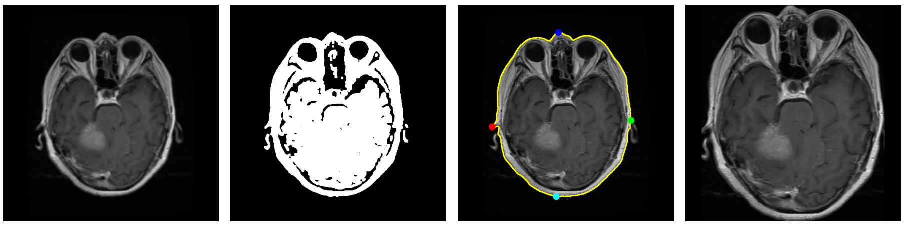

(a) (b) (c) (d)

Fig. 2 Pre-processing steps: (a) Blurred image; (b) Thresholded image; (c) Extreme points; (d) Cropped image.

3.3 Method overview

The proposed method consists mainly on applying some of the percolation concepts defined in [27]. First, the gliding-box algorithm is applied to the input image. It involves placing a box of size $L \times L$ on the upper-left corner of the image and then, moving it one pixel at a time until it reaches the bottom-right corner. At each iteration, a pixel similarity analysis is performed on the area covered by the box. The analysis is performed by comparing the intensity level of the central pixel F_c with that of each pixel F_i in the box using the chessboard distance Δ, given by Equation 1:

$$\Delta = max(|F_i - F_c|). \tag{1}$$

Then, the obtained Δ is compared to the value of L. If $\Delta \leq L$ then the box is labeled as 1, otherwise, it is labeled as 0. This procedure generates a binary matrix for each box, wherein the pixels labeled as 1 are considered pores. Following this step, we check which boxes match the percolation threshold criteria. This is done by evaluating the ratio of the number of pixels labeled as pores, given by Ω, to the total number of pixels in the box, given by L^2. If this value is greater than or equal to the threshold for square matrices (0.59275, [27, 29]), the value 1 is assigned to the box and 0 otherwise. These values are then used to generate a binary mask representing the percolation properties of the input image at the L scale. Since the input image has a resolution of $H \times W$, the mask size S for a scale L is given by Equation 2:

$$S(L) = (H - \frac{L-1}{2}) \times (W - \frac{L-1}{2}). \tag{2}$$

Then, the input image is cropped to match the resolution of the mask. Next, an element-wise multiplication is performed between the input image and the complement image of the mask. This results in a percolation image. In Figure 3, some examples of the obtained masks and their respective percolation images are shown, considering $L = 3$. The next step of the proposed method consists in classifying the input and percolation images with a CNN.

3.4 Classification

The images are classified through a ResNet-50 CNN. We have chosen this model as it has shown the best balance between performance and computing cost in preliminary tests. In this stage, both the input and percolation images are given as input to a pre-trained ResNet-50 model. The classifications are done separately, which means that results obtained for each image are independent. After performing classifications, the scores (i.e. class probability distributions) obtained from the softmax layers of each CNN are combined by the sum rule. After this summation, the class with the highest score is considered the predicted class. An overview of the proposed method is shown in Fig 4.

3.5 Performance evaluation

The performance of the proposed method was investigated through the following experiments: First, different sets of percolation images are generated with varying L values. These sets are given as input to the ResNet-50 and the obtained results are evaluated, aiming to verify how the choice of different scales for the gliding-box algorithm affects the performance. Then, the original image is also classified, and resulting scores are combined with the ones generated

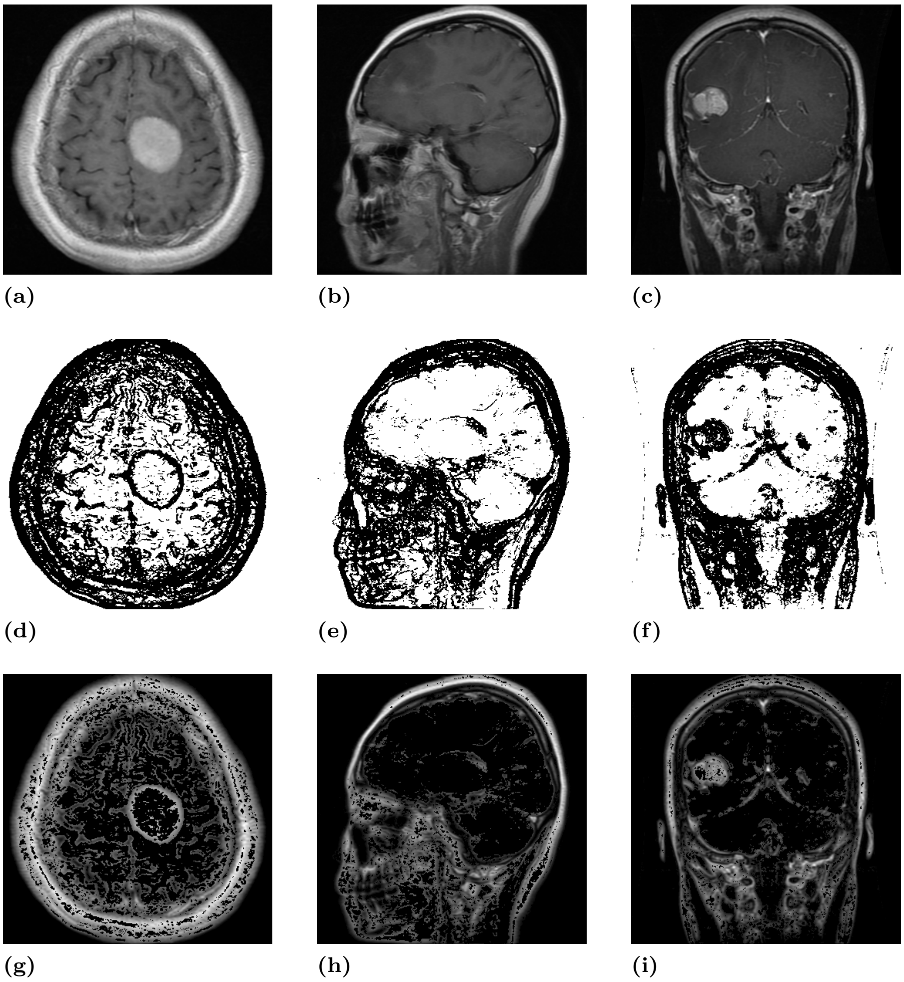

Fig. 3 (a), (b) and (c): Original images; (d), (e) and (f): masks obtained from applying the proposed method on the images (a), (b) and (c), respectively, with a scale of $L = 3$; (g), (h) and (i): percolation images obtained from the multiplication of the masks with their respective input images.

by the classification of the percolation image sets. Next, the results are compared to the ones obtained by traditional feature extraction and classification approaches.

We have also evaluated the classification performance of each of three available perspectives separately. The dataset was split into three sub-groups: sagittal; coronal; and axial. The procedures applied for training and classification of the full dataset were also applied for evaluating the sub-groups. In Fig. 5, an example from each point-of-view available is shown.

The extraction of the percolation features, the generation of the masks and percolation images, as well as the CNN classifications were all performed in Matlab R2019b. All tests were run on a *Intel Xeon Silver 4116 CPU* of

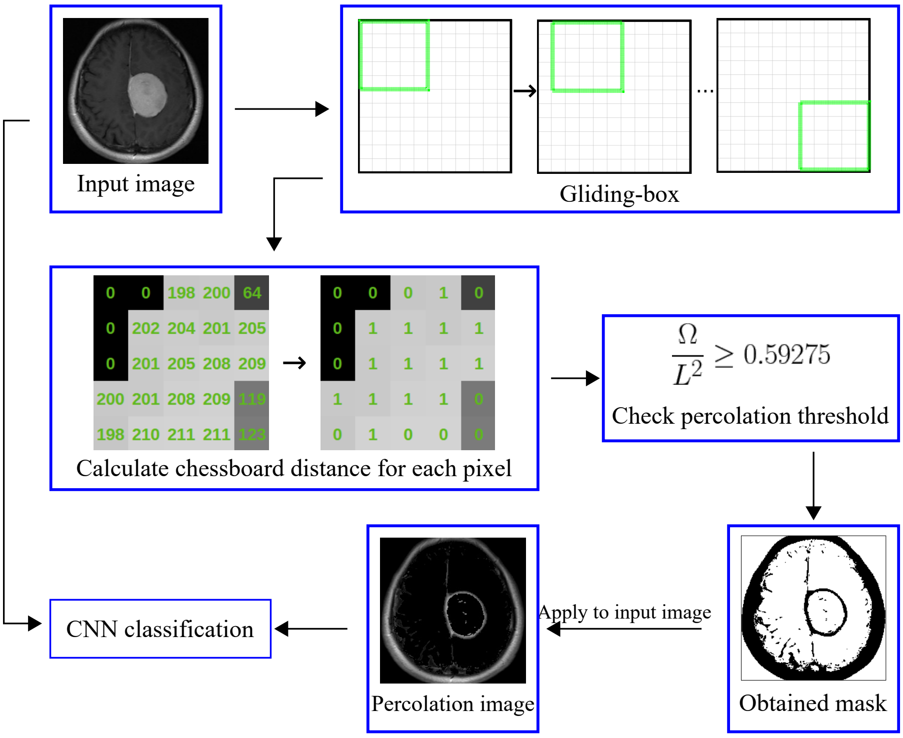

Fig. 4 Overview of the proposed method.

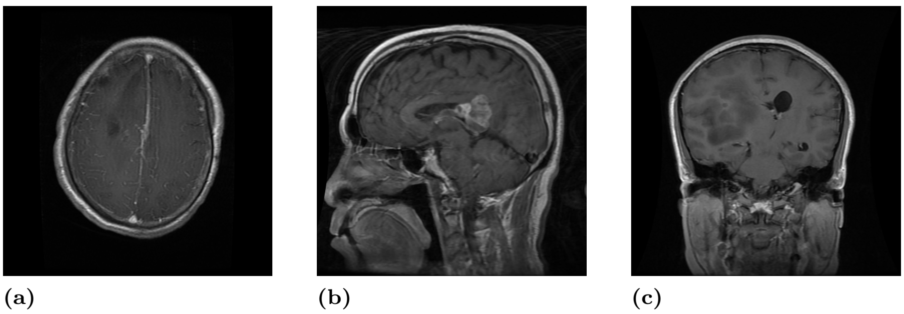

Fig. 5 Examples of the three available views: (a) Axial; (b) Sagittal; (c) Coronal.

2.10GHz, 128GB RAM and a *NVIDIA GeForce RTX 2080Ti* card. The Five-fold cross-validation technique with was adopted in all test steps to avoid problems such as *overfitting*. For training the CNN models, the default values of hyper-parameters available from the *Deep Learning Toolbox* of the *software MATLAB R2019b* were used, which are an initial learning rate of 0.01; a learning rate drop period of 2 epochs; a learning rate drop factor of 0.75; a mini-batch size of 32; an L2 regularization of 0.0001 and using solver sgdm with 10 training epochs.

4 Results and Discussion

The first experiments consisted on evaluating the performance of the generated percolation images across different scales. The values chosen for evaluation were $L = 3, 7, 11, 15, 19, 23, 27$. The results obtained for all evaluated scenarios are shown in Table 1.

Table 1 Performance of the percolation images with different scales.

	Full dataset	Axial	Sagittal	Coronal
$L = 3$	**91.45%**	89.22%	86.43%	88.33%
$L = 7$	91.02%	**90.13%**	**89.18%**	89.56%
$L = 11$	91.22%	88.72%	88.50%	**91.18%**
$L = 15$	90.67%	88.52%	88.30%	90.42%
$L = 19$	89.52%	85.30%	87.02%	88.90%
$L = 23$	89.36%	85.90%	86.33%	90.42%
$L = 27$	88.54%	84.79%	85.25%	90.32%

When the full dataset is considered, the best performance was obtained with a scale value of $L = 3$, with an accuracy value of 91.45%. With an exception for the scale $L = 11$, the classification performance gradually deteriorates as the scale increases. This trend is also observed for the classification of subgroups representing axial and sagittal views, where the lowest accuracy values occurred at the highest L values. The best accuracy value for these two subgroups was obtained at $L = 7$. For the coronal subgroup, larger L scales perform better than for the other subgroups. We believe this may indicate that the images obtained from this viewpoint do not contain relevant information at the borders, because the larger the scale, the more border pixels are cropped from the input image, to fit the mask resolution. The second stage of experiments was to evaluate the CNN ensembles considering the classification of the original and percolation images, combined by the sum rule. The results are shown in Table 2.

For the classification of the entire dataset, the best result was an accuracy rate of 94.22%, which was obtained in the ensemble composed by the original images and the percolation images generated at a scale of $L = 3$. This represents an improvement of 0.59% over the classification accuracy of the original images alone. For the classification of the three subgroups represented by each

Table 2 Performance of the ensemble composed by the classification of the input and percolation images.

	Full dataset	Axial	Sagittal	Coronal
Original image	93.83%	92.25%	90.86%	92.79%
Original + Percolation image ($L = 3$)	**94.42%**	92.04%	91.15%	92.22%
Original + Percolation image ($L = 7$)	94.22%	**93.05%**	**92.43%**	**93.64%**
Original + Percolation image ($L = 11$)	94.06%	91.44%	**92.43%**	93.07%
Original + Percolation image ($L = 15$)	93.77%	91.24%	91.84%	93.45%
Original + Percolation image ($L = 19$)	93.28%	91.14%	91.64%	92.60%
Original + Percolation image ($L = 23$)	93.64%	91.84%	90.86%	92.60%
Original + Percolation image ($L = 27$)	93.31%	89.93%	90.86%	93.17%

of the different perspectives, the best results were obtained in the ensemble composed by the percolation images generated with a scale of $L = 7$. In these four scenarios, the inclusion of a CNN for classifying the percolation images improved the accuracy obtained. The best improvement was observed in the classification of the sagittal sub-group, where accuracy increased by 1.57%. We also analyzed the preformance of the individual classes using other metrics besides accuracy, such as sensitivity (true positive rate), specificity (true negative rate) and F1-score. The results are shown in Tables 3 through 6. The confusion matrix for the full dataset classification is shown in Table 7. The pituitary class performed best in the classifications using the full dataset and in the scenarios related to the sagittal and coronal view classification. For the axial view, the best performance was obtained by the glioma class. The meningioma class provided the lowest metrics in all scenarios, indicating greater difficulty in performing the classification.

Table 3 Performance measures for the full dataset using the proposed ensemble with $L = 7$.

Class	Accuracy	Sensitivity	Specificity	F1-score
Meningioma	94.75%	0.872	0.970	0.885
Glioma	96.31%	0.960	0.966	0.960
Pituitary	97.39%	0.969	0.976	0.956

Table 4 Performance measures for the Axial images using the proposed ensemble with $L = 7$.

Class	Accuracy	Sensitivity	Specificity	F1-score
Meningioma	94.26%	0.841	0.969	0.860
Glioma	96.17%	0.964	0.960	0.962
Pituitary	95.67%	0.938	0.964	0.927

To test how our approach compares with other traditional feature extraction techniques in computer vision, we obtained LBP, Haralick, and fractal descriptors from the original images and gave them as input to a Random

Table 5 Performance measures for the Sagittal images using the proposed ensemble with $L = 7$.

Class	Accuracy	Sensitivity	Specificity	F1-score
Meningioma	94.00%	0.899	0.955	0.888
Glioma	94.30%	0.919	0.961	0.932
Pituitary	96.56%	0.953	0.971	0.945

Table 6 Performance measures for the Coronal using the proposed ensemble with $L = 7$.

Class	Accuracy	Sensitivity	Specificity	F1-score
Meningioma	94.12%	0.879	0.959	0.868
Glioma	95.26%	0.942	0.962	0.950
Pituitary	97.91%	0.969	0.984	0.966

Table 7 Confusion matrix for the full dataset using the proposed ensemble with $L = 7$.

		Actual class		
		Meningioma	Glioma	Pituitary
Predicted as	Meningioma	**617**	53	17
	Glioma	44	**1369**	12
	Pituitary	47	4	**901**

Forest classifier, using the same Five-fold partitioning used in previous experiments. The comparison is shown in Table 8. It can be noted that the proposed method significantly outperforms the other techniques, even when only the percolation images are given as input to the CNN. This indicates that our proposal is a promising approach, and we believe that it may be able to fill the gap related to the classification of MRI datasets using percolation concepts.

Table 8 Accuracy values obtained by different computer vision methods.

	Full dataset	Axial	Sagittal	Coronal
LBP	68.70%	72.41%	60.28%	72.39%
Haralick	74.45%	75.53%	73.75%	77.89%
Fractals (FD, LAC and percolation)	72.55%	75.73%	72.47%	75.14%
ResNet-50 (original image)	93.83%	92.25%	90.86%	92.79%
ResNet-50 (percolation image, $L = 7$)	91.02%	90.13%	89.18%	89.56%
Proposed (ensemble, L=7)	**94.22%**	**93.05%**	**92.43%**	**93.64%**

5 Conclusion

In this paper, we proposed an approach to extract percolation features from brain MRI images and then generate a mask, in order to apply it to the original images and obtain a percolation image. Both the original image and percolation image were given as input to a CNN ensemble and accuracy values of up to 94.42% were obtained. The percolation image can be obtained using different scales. We evaluated seven possible scale values and observed that smaller values tend to provide slightly better results. We also evaluated the classification of sub-groups composed by images obtained only from a given perspective: axial; sagittal; or coronal. Our proposed ensemble outperformed the standard CNN classification and other computer vision approaches evaluated in all scenarios tested using a scale of $L = 7$.

We believe this is a promising approach, which can be further explored to provide contributions to research regarding classification of MRI datasets using percolation concepts. For future work, we propose the evaluation of different datasets and CNN models, in addition to the Resnet50. We also consider the inclusion of other percolation properties, such as number of percolating clusters per box and size of the largest cluster, in the percolation image generation process.

Acknowledgements This study was financed in part by the Coordenação de Aperfeiçoamento de Pessoal de Nível Superior - Brasil (CAPES) - Finance Code 001 and by the Programa Institucional de Internacionalização (PRINT/CAPES, Brazil), project #88882.461704/2019-01. The authors gratefully acknowledge the financial support of National Council for Scientific and Technological Development CNPq (Grant #311404/2021-9, Grant #313643/2021-0) and the State of Minas Gerais Research Foundation - FAPEMIG (Grant #APQ-00578-18 and Grant #APQ-01129-21).

Conflict of interest

The authors declare that they have no conflict of interest.

References

1. Louis DN, Perry A, Wesseling P, Brat DJ, Cree IA, Figarella-Branger D, Hawkins C, Ng HK, Pfister SM, Reifenberger G, Soffietti R, von Deimling A, Ellison DW (2021) The 2021 WHO classification of tumors of the central nervous system: a summary. Neuro Oncol 23(8):1231–1251
2. Abir TA, Siraji JA, Ahmed EU (2018) Analysis of a novel mri based brain tumour classification using probabilistic neural network (pnn). International journal of scientific research in science, engineering and technology 4:69–75
3. Yaseen S, Al-Araji A, Humaidi A (2022) Brain tumor segmentation and classification: A one-decade review. International Journal of Nonlinear Analysis and Applications pp –, DOI 10.22075/ijnaa.2022.27445.3601, URL `https://ijnaa.semnan.ac.ir/article_6595.html`, `https://ijnaa.semnan.ac.ir/article_6595_631616daa3ddfa8ca2300131b0ebd099.pdf`
4. Rehman A, Naz S, Razzak MI, Akram F, Imran M (2020) A deep learning-based framework for automatic brain tumors classification using transfer learning. Circuits, Systems, and Signal Processing 39(2):757–

775, DOI 10.1007/s00034-019-01246-3, URL https://doi.org/10.1007/s00034-019-01246-3

5. Nayak DR, Padhy N, Mallick PK, Zymbler M, Kumar S (2022) Brain tumor classification using dense efficient-net. Axioms 11(1), DOI 10.3390/axioms11010034, URL https://www.mdpi.com/2075-1680/11/1/34
6. Sachdeva J, Kumar V, Gupta I, Khandelwal N, Ahuja CK (2016) A package-sfercb-"segmentation, feature extraction, reduction and classification analysis by both svm and ann for brain tumors". Applied Soft Computing 47:151–167, DOI https://doi.org/10.1016/j.asoc.2016.05.020, URL https://www.sciencedirect.com/science/article/pii/S1568494616302216
7. Sharma Y, Chhabra M (2015) An improved automatic brain tumor detection system. International Journal of Advanced Research in Computer Science and Software Engineering 5(4):11–15
8. Iftekharuddin KM, Zheng J, Islam MA, Ogg RJ (2009) Fractal-based brain tumor detection in multimodal mri. Applied Mathematics and Computation 207(1):23–41, DOI https://doi.org/10.1016/j.amc.2007.10.063, URL https://www.sciencedirect.com/science/article/pii/S0096300308000179, includes Special issue on Emergent Applications of Fractals and Wavelets in Biology and Biomedicine
9. Cheng J, Huang W, Cao S, Yang R, Yang W, Yun Z, Wang Z, Feng Q (2015) Enhanced performance of brain tumor classification via tumor region augmentation and partition. PLOS ONE 10(10):1–13, DOI 10.1371/journal.pone.0140381, URL https://doi.org/10.1371/journal.pone.0140381
10. Ullah N, Khan JA, Khan MS, Khan W, Hassan I, Obayya M, Negm N, Salama AS (2022) An effective approach to detect and identify brain tumors using transfer learning. Applied Sciences 12(11), DOI 10.3390/app12115645, URL https://www.mdpi.com/2076-3417/12/11/5645
11. Swati ZNK, Zhao Q, Kabir M, Ali F, Ali Z, Ahmed S, Lu J (2019) Brain tumor classification for mr images using transfer learning and fine-tuning. Computerized Medical Imaging and Graphics 75:34–46, DOI https://doi.org/10.1016/j.compmedimag.2019.05.001, URL https://www.sciencedirect.com/science/article/pii/S0895611118305937
12. Badža MM, Barjaktarović MC (2020) Classification of brain tumors from mri images using a convolutional neural network. Applied Sciences 10(6), DOI 10.3390/app10061999, URL https://www.mdpi.com/2076-3417/10/6/1999
13. Mzoughi H, Njeh I, Wali A, Slima MB, BenHamida A, Mhiri C, Mahfoudhe KB (2020) Deep multi-scale 3d convolutional neural network (cnn) for mri gliomas brain tumor classification. Journal of Digital Imaging 33(4):903–915, DOI 10.1007/s10278-020-00347-9, URL https://doi.org/10.1007/s10278-020-00347-9
14. Díaz-Pernas FJ, Martínez-Zarzuela M, Antón-Rodríguez M, González-Ortega D (2021) A deep learning approach for brain tumor classifica-

tion and segmentation using a multiscale convolutional neural network. Healthcare 9(2), DOI 10.3390/healthcare9020153, URL https://www.mdpi.com/2227-9032/9/2/153
15. Kokkalla S, Kakarla J, Venkateswarlu IB, Singh M (2021) Three-class brain tumor classification using deep dense inception residual network. Soft Computing 25(13):8721–8729, DOI 10.1007/s00500-021-05748-8, URL https://doi.org/10.1007/s00500-021-05748-8
16. Shaik NS, Cherukuri TK (2022) Multi-level attention network: application to brain tumor classification. Signal, Image and Video Processing 16(3):817–824, DOI 10.1007/s11760-021-02022-0, URL https://doi.org/10.1007/s11760-021-02022-0
17. El Kader IA, Xu G, Shuai Z, Saminu S (2021) Brain tumor detection and classification by hybrid cnn-dwa model using mr images. Current Medical Imaging 17(10):1248–1255
18. Alanazi MF, Ali MU, Hussain SJ, Zafar A, Mohatram M, Irfan M, Al-Ruwaili R, Alruwaili M, Ali NH, Albarrak AM (2022) Brain tumor/mass classification framework using magnetic-resonance-imaging-based isolated and developed transfer deep-learning model. Sensors 22(1), DOI 10.3390/s22010372, URL https://www.mdpi.com/1424-8220/22/1/372
19. Di Ieva A, Russo C, Liu S, Jian A, Bai MY, Qian Y, Magnussen JS (2021) Application of deep learning for automatic segmentation of brain tumors on magnetic resonance imaging: a heuristic approach in the clinical scenario. Neuroradiology 63(8):1253–1262, DOI 10.1007/s00234-021-02649-3, URL https://doi.org/10.1007/s00234-021-02649-3
20. Russo C, Liu S, Di Ieva A (2021) Spherical coordinates transformation pre-processing in deep convolution neural networks for brain tumor segmentation in MRI. Med Biol Eng Comput 60(1):121–134
21. Cheng J (2017) brain tumor dataset. DOI 10.6084/m9.figshare.1512427.v5, URL https://figshare.com/articles/dataset/brain_tumor_dataset/1512427
22. Sartaj B, Ankita K, Prajakta B, Dedge S, Kanchan S (2020) Brain tumor classification (mri). Data retrieved from Kaggle, https://www.kaggle.com/datasets/sartajbhuvaji/brain-tumor-classification-mri
23. Roberto GF, Neves LA, Nascimento MZ, Tosta TA, Longo LC, Martins AS, Faria PR (2017) Features based on the percolation theory for quantification of non-hodgkin lymphomas. Computers in biology and medicine 91:135–147
24. Baish JW, Jain RK (2000) Fractals and cancer. Cancer research 60(14):3683–3688
25. Roberto GF, Nascimento MZ, Martins AS, Tosta TA, Faria PR, Neves LA (2019) Classification of breast and colorectal tumors based on percolation of color normalized images. Computers & Graphics 84:134–143
26. de Meneses FGA, Lima GD, Nunes M, Bastos VH, Teixeira S (2019) Percolation theory for the recognition of patterns in topographic images of the cortical activity. Medical Hypotheses 125:37–40

27. Roberto GF, Lumini A, Neves LA, do Nascimento MZ (2021) Fractal neural network: A new ensemble of fractal geometry and convolutional neural networks for the classification of histology images. Expert Systems with Applications 166:114103
28. Kang J, Ullah Z, Gwak J (2021) Mri-based brain tumor classification using ensemble of deep features and machine learning classifiers. Sensors 21(6), DOI 10.3390/s21062222, URL `https://www.mdpi.com/1424-8220/21/6/2222`
29. Bird N, Perrier E (2010) Multiscale percolation properties of a fractal pore network. Geoderma 160(1):105–110, URL `https://doi.org/10.1016/j.geoderma.2009.10.009`